

## *Electronic Supplementary Information*

### **NO<sub>x</sub> reduction against sulfur poisoning by using Ce modified Cu-SAPO-34 catalysts**

*Liumei Ge, Aiyong Wang, Xiaonan Hu, Jin Zhang, Jiebing He, Penglu Wang, Lupeng Han, Dengsong Zhang\**

*State Key Laboratory of Advanced Special Steel, School of Environmental and Chemical Engineering, International Joint Laboratory of Catalytic Chemistry, College of Sciences, Shanghai University, Shanghai 200444, China.*

*\*To whom correspondence should be addressed:*

E-mail: [dszhang@shu.edu.cn](mailto:dszhang@shu.edu.cn).

## Catalyst preparation

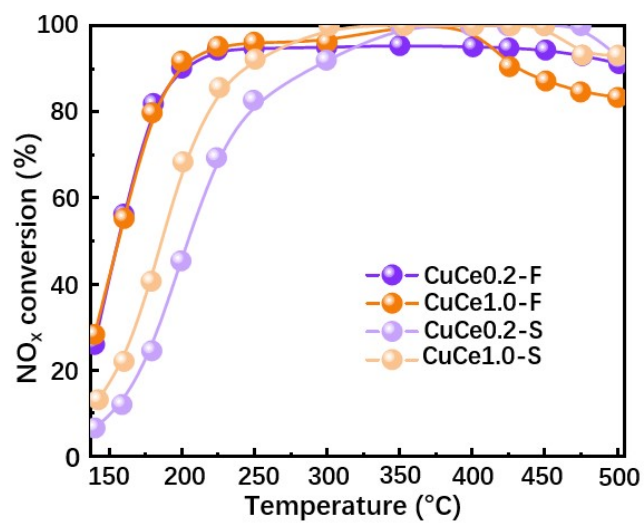
Different mass contents of Ce were introduced into Cu-SAPO-34 by wet impregnation method. First, different masses of  $\text{Ce}(\text{NO}_3)_3 \cdot 6\text{H}_2\text{O}$  corresponding the contents of 0.2 wt.%, 0.5 wt.% and 1.0 wt.% Ce were weighed and dissolved in 35 mL of deionized water, respectively. Then added 1 g Cu-SAPO-34 to the each of the solutions and stirred well. The vacuum rotary evaporator was used to evaporate the mixture at 60 °C, dried overnight, and the calcined at 500 °C for 4 h, heating rate was 2 °C /min, which were denoted as  $\text{CuCe}_x\text{-F}$  ( $x=0.2, 0.5, 1.0$ , represent Cu-SAPO-34 theoretically containing 0.2 wt.%, 0.5 wt.%, 1.0 wt.% of Ce content by mass, respectively).

## Characterization

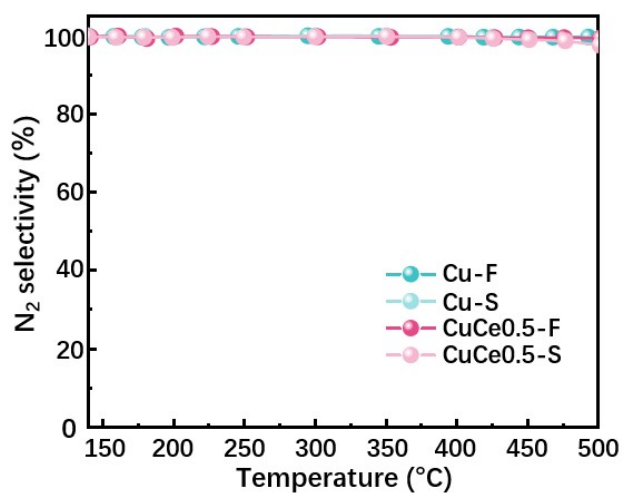
Scanning electron microscope pictures were obtained by a field emission scanning electron microscopy (FE-SEM, Sigma-300) and element distribution were collected by Energy Dispersive Spectroscopy (EDS). The X-ray diffraction (XRD) tests were explored by Bruker D8 Advance diffractometer equipped with a  $\text{Cu K}\alpha$  (40 kV, 40 mA) radiation source and a LynxEye\_XE-T linear detector, and the XRD patterns were recorded in the  $2\theta$  range of 5-50° at a scanning speed of 0.02° s<sup>-1</sup>. The Raman spectra were carried out on the LabRAM HR Evolution (Horiba) with a laser of 532 nm. The spectra were obtained in the range of 200-1200 cm<sup>-1</sup> and the spectral resolution employed was 4 cm<sup>-1</sup>. Nitrogen adsorption-desorption experiments were measured on the Micromeritics ASAP 2020 instrument, and the specific surface area was calculated by the Brunauer-Emmett-Teller (BET) method. The catalysts were outgassed at 200 °C for 12 h before the experiments. The temperature-programmed desorption (TPD) experiments of  $\text{NH}_3$  with Mass Spectrometry (OMNISTAR) ( $\text{NH}_3$ -TPD-MS) were

carried out on the Micromeritics Auto Chem HP 2920. Before the NH<sub>3</sub>-TPD-MS experiments, 80 mg of samples were pre-treated with 2% O<sub>2</sub>/He protection (30 mL/min) at 300 °C for 30 min and then cooled to 100 °C, then purged the pipe with He atmosphere for 10 min. Catalysts were exposed to 10% NH<sub>3</sub>/He for 1 h at 100 °C, the physical adsorption of ammonia was removed by He purging for 1 h at the same temperature. In the end, the temperature was raised to 900 °C with a ramping rate of 10 °C/min. The UV-vis absorbance was completed by diffuse reflectance spectra (DRS) using UV-vis spectrophotometer (Agilent Cary 5000 UV-vis-DRS spectrometer) and BaSO<sub>4</sub> was used as reference standard. Spectra were measured between 200 and 1000 nm with a data interval of 1 nm and at a rate of 200 nm/min. Inductively coupled plasma optical emission spectroscopy (ICP-OES) was tested the elemental content using an Agilent 5110 of the US, and before the experiment, the 10 mg catalysts were dissolved in hydrofluoric acid. Temperature-programmed reduction experiment of H<sub>2</sub> (H<sub>2</sub>-TPR) was carried out to reveal the redox ability of samples on Micromeritics Auto Chem HP 2920. Before the H<sub>2</sub>-TPR experiments, 80 mg of each sample was treated under 2% O<sub>2</sub>/He atmosphere with a flow rate of 30 mL/min at 300 °C for 30 min, then cooled to room temperature under 2% O<sub>2</sub>/He atmosphere. And then the pipe was purged with He atmosphere, in order to remove the O<sub>2</sub> from the pipe. During the H<sub>2</sub>-TPR experiment, the catalysts were exposed to 10% H<sub>2</sub>/Ar and then the reactor temperature was raised 900 °C with a rate of 10 °C/min. *In situ* diffuse reflectance infrared fourier transform (*In situ* DRIFT) spectroscopy was completed using a NicoSUANlet 6700 spectrometer to study the adsorption behaviors between NO<sub>x</sub> and NH<sub>3</sub> over each catalyst and mechanism of the transient reaction. All DRIFT spectra were collected in the wavenumber range of 4000 cm<sup>-1</sup> to 750 cm<sup>-1</sup> in the Kubelka-Munk format, accumulating 64 scans per minute at 4 cm<sup>-1</sup> resolution. Prior to each measurement,

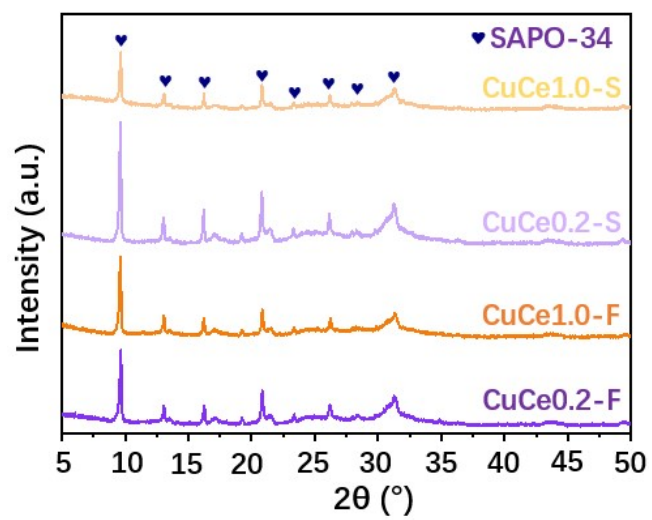
every catalyst was pre-treated at 300 °C under Ar+O<sub>2</sub> mixed flow for 30 min, and then regulated to the target temperature to obtain a background spectrum which should be deducted from the sample spectra. Moreover, for the transient reaction between NO+O<sub>2</sub> (NH<sub>3</sub>) and pre-adsorbed NH<sub>3</sub> (or NO+O<sub>2</sub>), after the same pretreatment, the samples were exposed 500 ppm of NH<sub>3</sub> (or NO+O<sub>2</sub>) for the adsorption at 200 °C. After 1 h, the catalysts were switch to a flow of NO+O<sub>2</sub> (or NH<sub>3</sub>) and meanwhile the reaction process was recorded as a function of time.



**Fig. S1.** Plots of NO<sub>x</sub> conversion versus temperature over CuCe0.2-F, CuCe1.0-F, CuCe0.2-S and CuCe1.0-S catalysts.

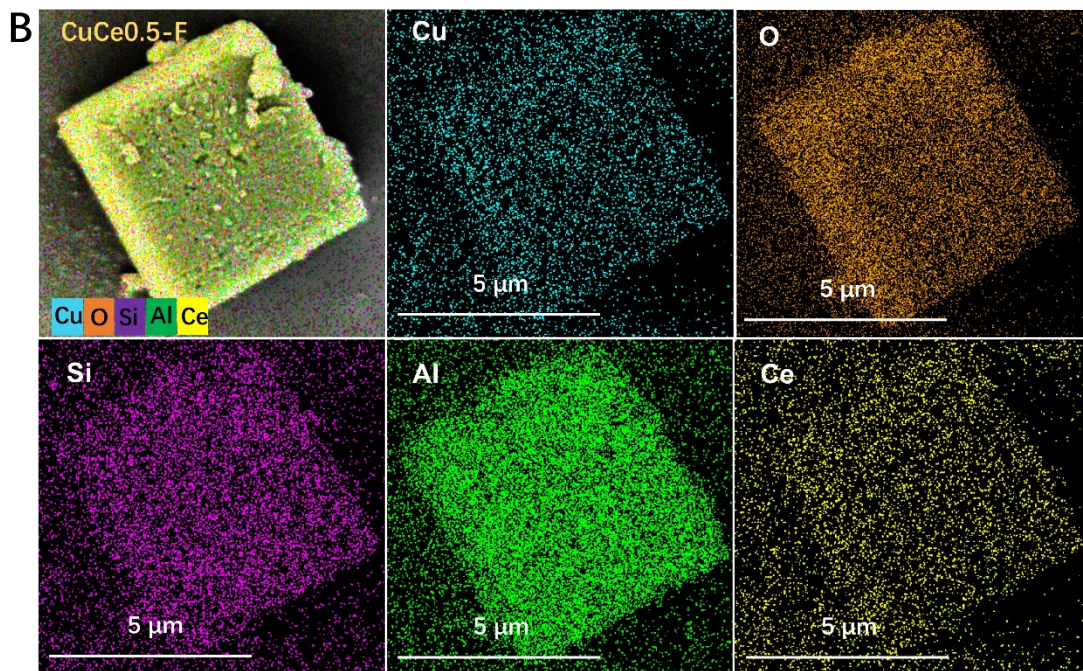
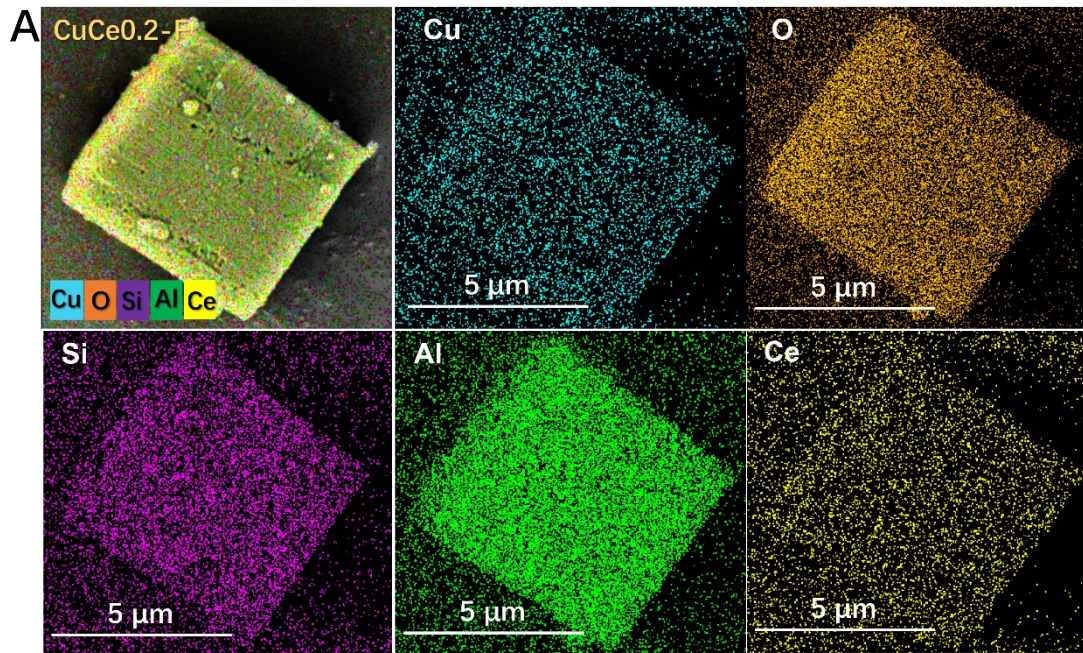


**Fig. S2.** Plot shows the N<sub>2</sub> selectivity over Cu-F, CuCe0.5-F, Cu-S and CuCe0.5-S. Reaction conditions: 500 ppm of NH<sub>3</sub>, 500 ppm of NO, 5 vol.% of O<sub>2</sub>, 2.5 vol.% of H<sub>2</sub>O balanced with N<sub>2</sub>, and 100,000 h<sup>-1</sup> of GHSV.

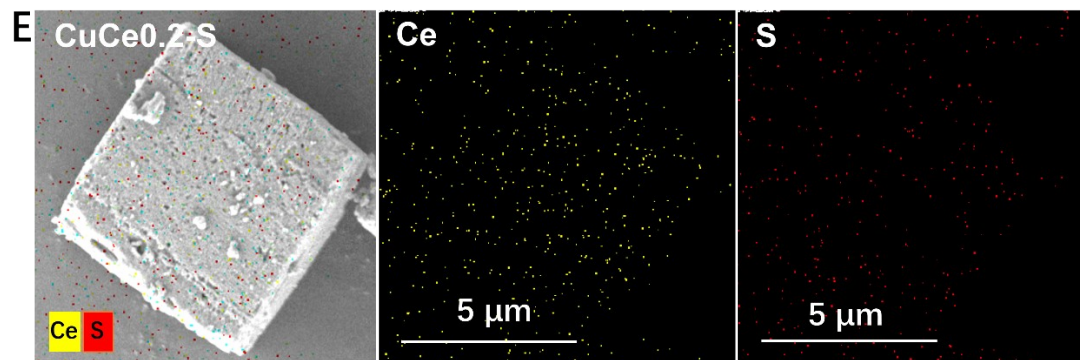
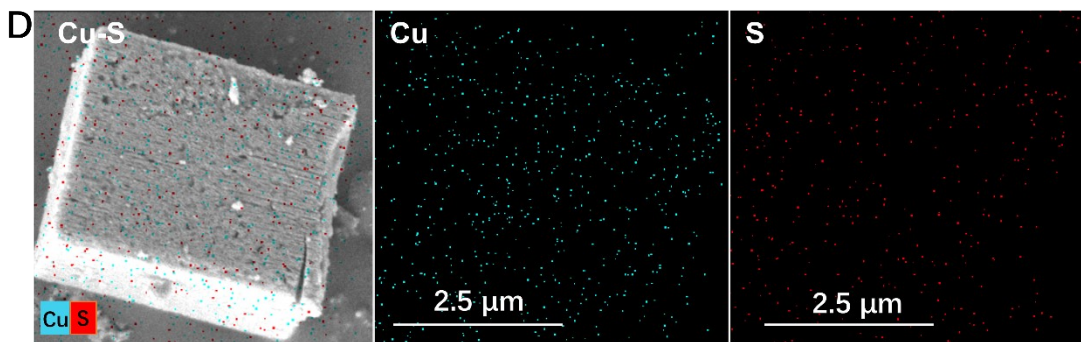
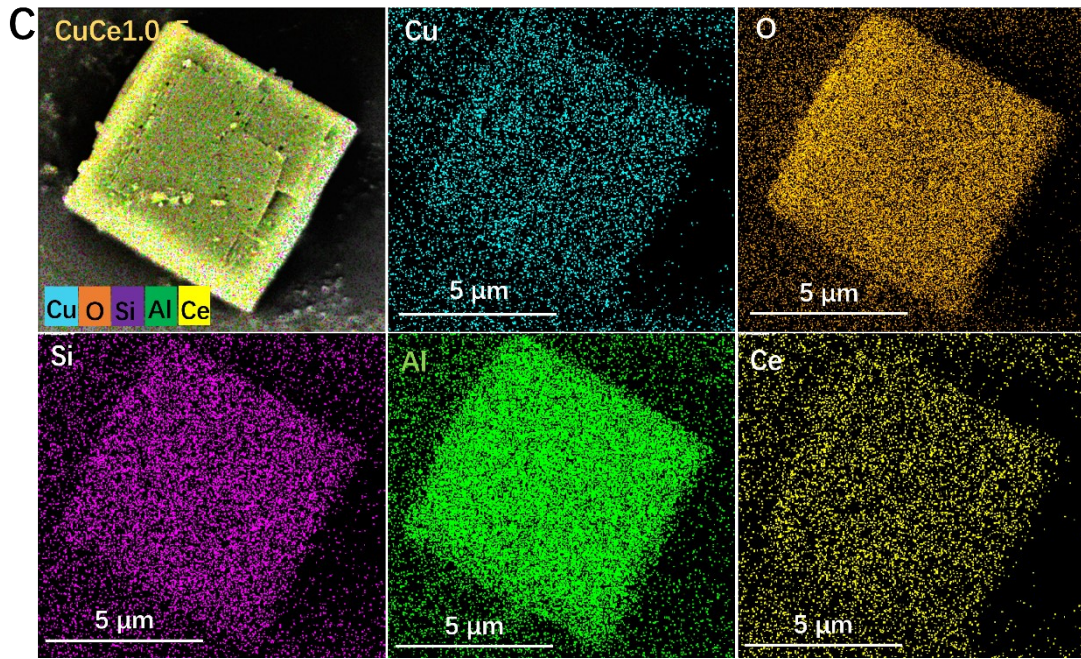


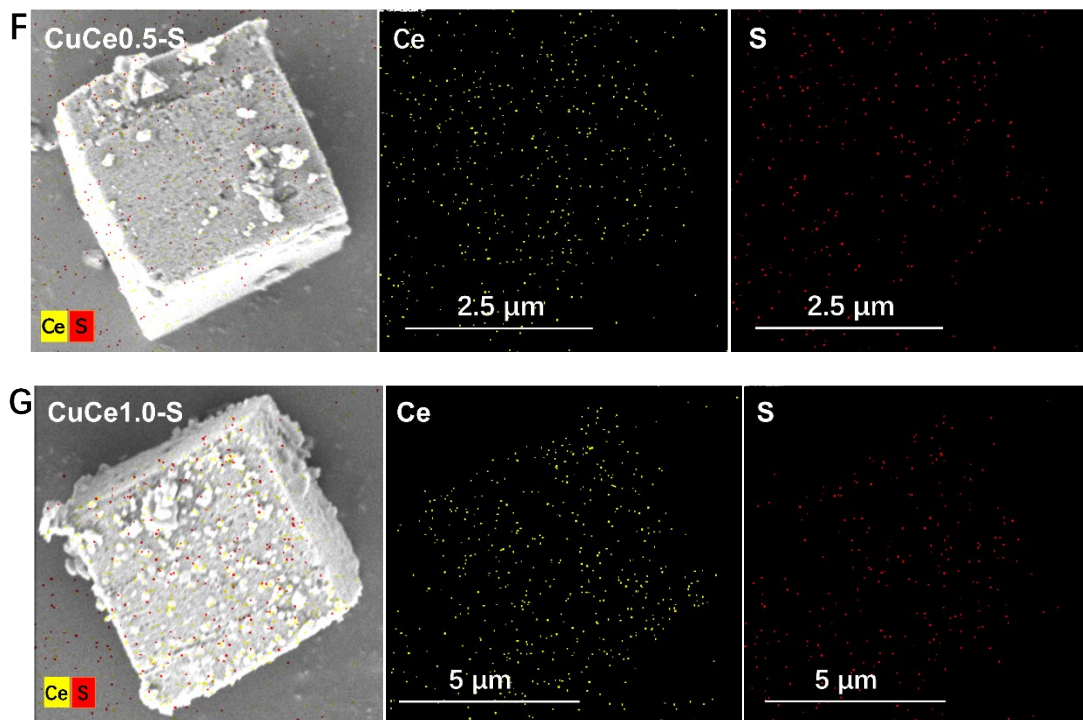
**Fig. S3.** XRD patterns of CuCe0.2-F, CuCe1.0-F, CuCe0.2-S and CuCe1.0-S.



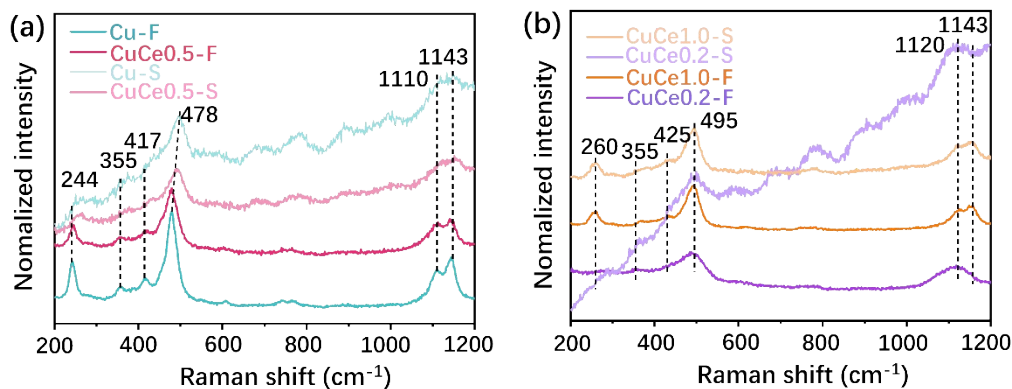






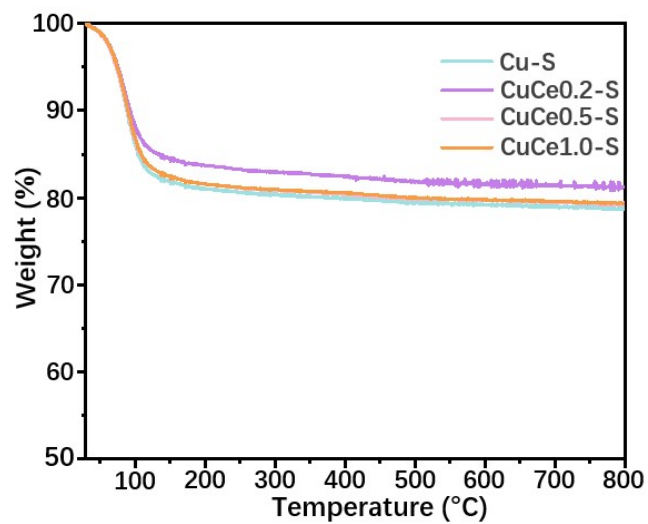


**Fig. S4.** SEM-EDS mapping of CuCe0.2-F (A), CuCe0.2-F (B), CuCe1.0-F (C), Cu-S (D), CuCe0.2-S (E), CuCe0.5-S (F), CuCe1.0-S (G).

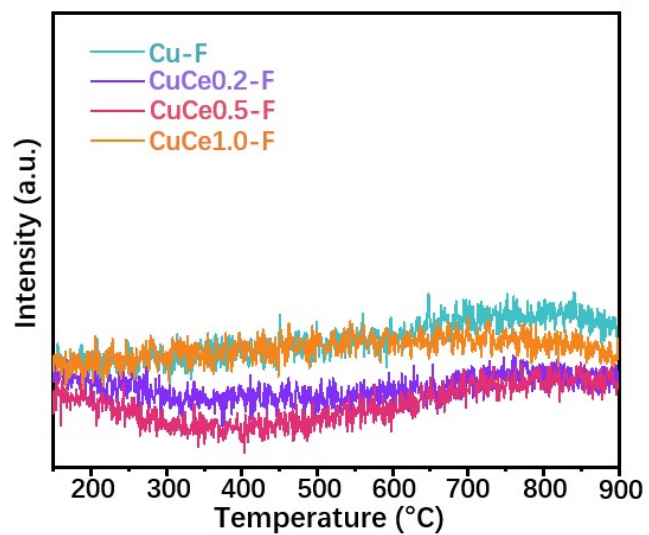


**Fig. S5.** Raman spectra of (a) Cu-F, CuCe0.5-F, Cu-S, CuCe0.5-S, (b) CuCe0.2-F, CuCe0.2-S, CuCe1.0-F and CuCe1.0-S.

Obviously, all the band intensities changed significantly after sulfur poisoning, and Cu-S experienced serious negative influence, while CuCe0.5-S and CuCe1.0-S catalysts suffered a slight decrease. Furthermore, peaks ( $244\text{ cm}^{-1}$  and  $478\text{ cm}^{-1}$ ) relating to the framework vibration of SAPO-34 over Cu-S catalyst appeared apparent change<sup>1,2</sup>, while CuCe0.5-S could maintain better signals. Besides, the band at  $355\text{ cm}^{-1}$  was assigned to the T-O-T (with T being Si or Al) ending vibration mode of six-membered ring (6MR)<sup>2</sup>. The peak of  $417\text{ cm}^{-1}$  was contributed to the Cu-O bending vibration mode. In addition, bands at  $1110\text{ cm}^{-1}$  and  $1143\text{ cm}^{-1}$  were assigned to the P-O-Al on Cu-SAPO-34<sup>2</sup>. Additionally, the diffraction peaks belong to  $\text{CuO}_x$  or  $\text{CeO}_2$  are not observed in the XRD patterns (Fig. 2a, Fig. S3), which means that the well distribution of Cu and Ce in the catalysts. Similarly, SEM-EDS mapping also proves Cu, O, Si and Al elements are uniformly distributed on the Cu-F catalyst (Fig.2b), and Fig. S4 exhibits that Ce and S well dispersion over the fresh and poisoned catalysts.

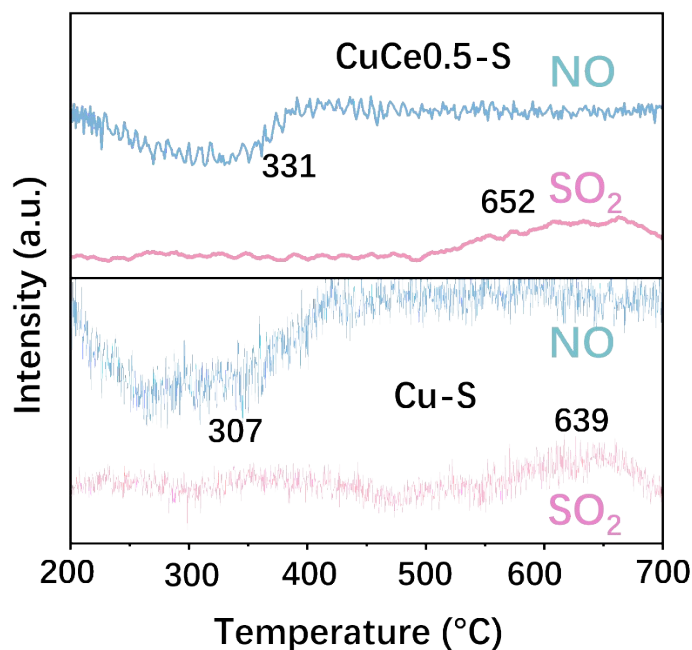


**Fig. S6.** TGA profiles of Cu-S, CuCe0.2-S, CuCe0.5-S and CuCe1.0-S



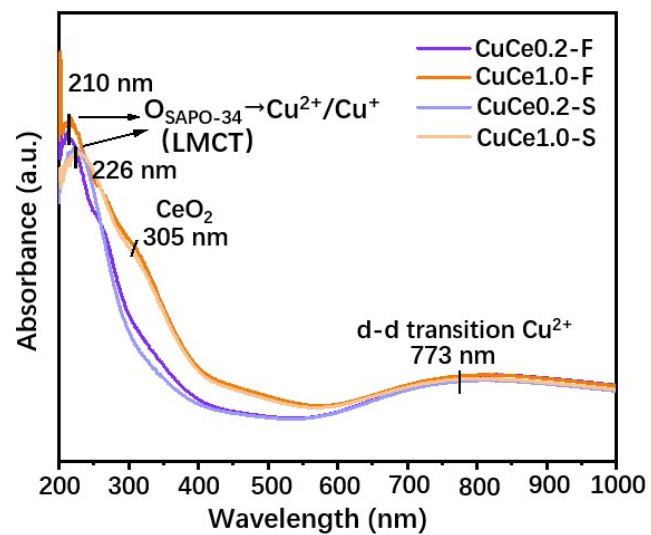
**Fig. S7.** SO<sub>2</sub>-TPD plots over Cu-F, CuCe0.2-F, CuCe0.5-F, CuCe1.0-F.





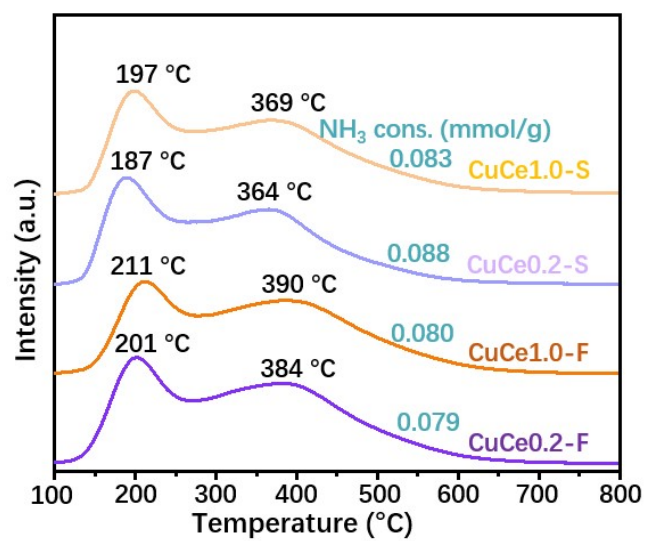
**Fig. S8.** TPSR profiles of Cu-S and CuCe0.5-S catalysts. Reaction conditions: 500 ppm of NO + 5 vol % O<sub>2</sub> in He at 30 mL/min; and heating rate of 4 °C/min.

Fig. S8 shows the TPSR data for Cu-S and CuCe0.5-S. As shown in the figure, the NO gas in both CuCe0.5-S and Cu-S catalysts went through a process of decreasing, then increasing and finally leveling off, and both reached the lowest NO concentration at 331 °C and 307 °C, respectively, indicating that NH<sub>3</sub> can be desorbed from the catalysts with increasing temperature and the NH<sub>3</sub>-SCR reaction occurs with the incoming NO, thus causing the NO concentration to decrease and then increase. However, no significant SO<sub>2</sub>-related peaks were observed in the range of 200-400 °C, indicating that the NH<sub>3</sub> reacting with NO in this range originated from the adsorption of the catalyst during the sulfidation process rather than from the decomposition of ABS on the catalyst. In addition, CuCe0.5-S and Cu-S showed SO<sub>2</sub> desorption peaks at 652 °C and 639 °C, respectively. The above results indicate that the S elements deposited on the sulfide samples are mainly in the form of metal sulfates, and the ABS content is so small that the SO<sub>2</sub> desorption signal is difficult to detect, as also illustrated by the SO<sub>2</sub>-TPD and TGA data.



**Fig. S9.** UV-vis-DRS spectra of CuCe0.2-F, CuCe0.2-S, CuCe1.0-F and CuCe1.0-S.





**Fig. S10.** NH<sub>3</sub>-TPD-MS profiles of CuCe0.2-F, CuCe0.2-S, CuCe1.0-F and CuCe1.0-S catalysts.

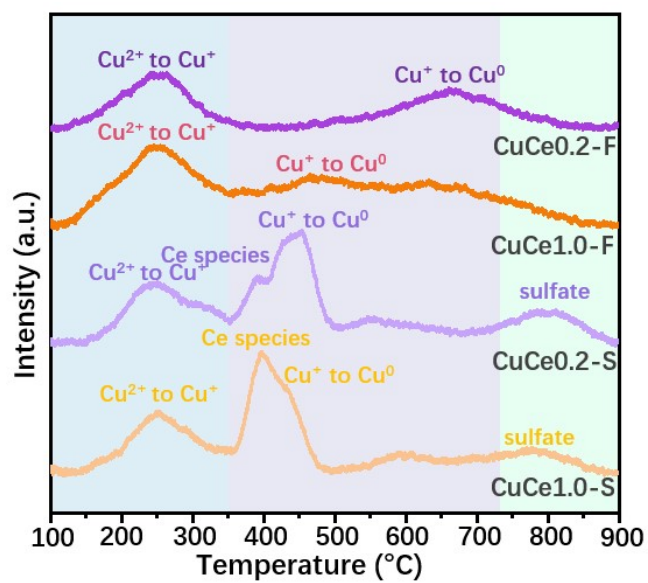


**Fig. S11.** H<sub>2</sub>-TPR profiles of CuCe0.2-F, CuCe1.0-F, CuCe0.2-S and CuCe1.0-S catalysts.

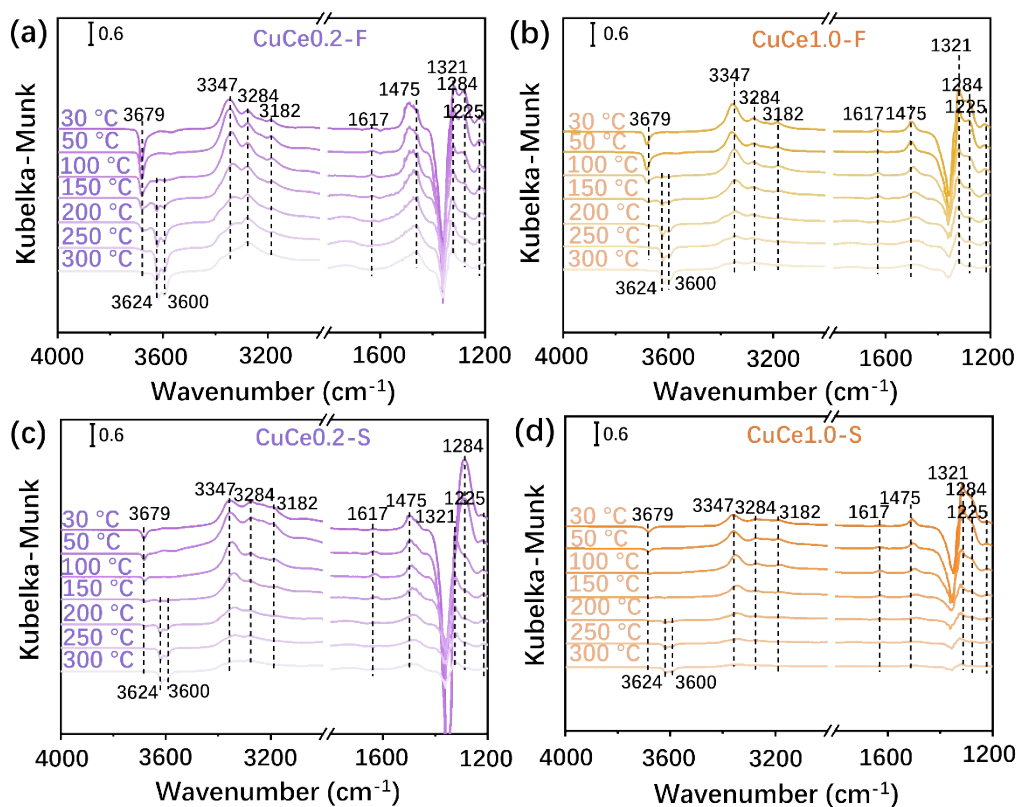


**Fig. S12.** In situ DRIFTS spectra of  $\text{NH}_3$  desorption over (a)  $\text{CuCe0.2-F}$ , (b)  $\text{CuCe1.0-F}$ , (c)  $\text{CuCe0.2-S}$  and (d)  $\text{CuCe1.0-S}$  catalysts.

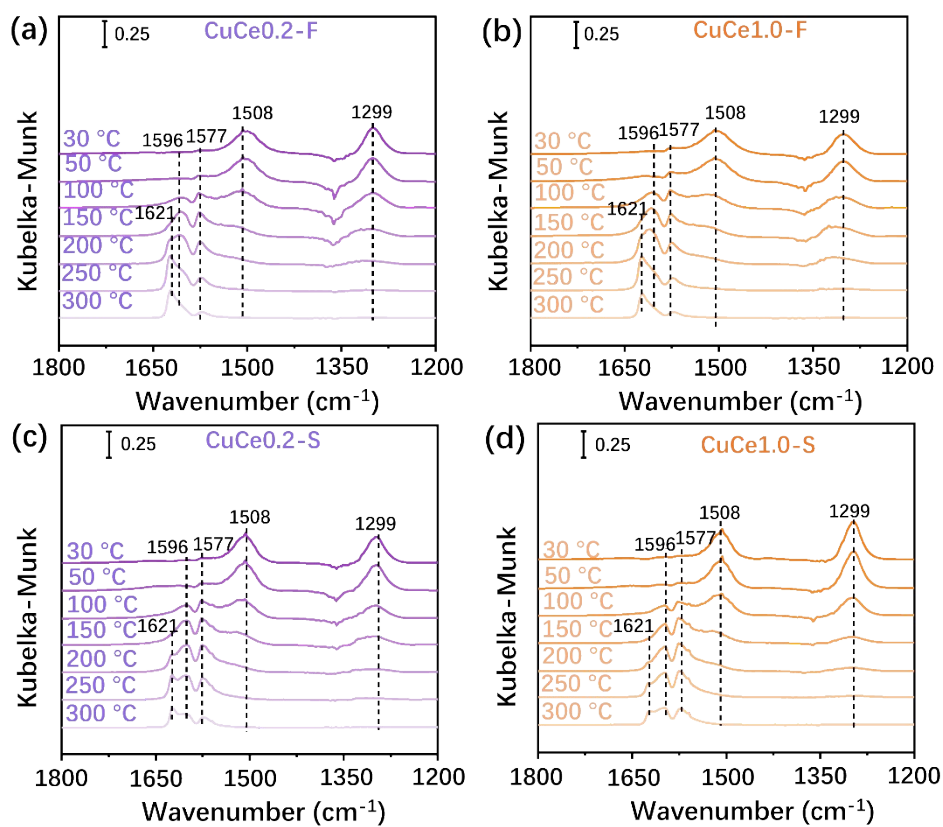


**Fig. S13.** In situ DRIFTS spectra of NO+O<sub>2</sub> co-desorption over (a)CuCe0.2-F, (b)CuCe1.0-F, (c)CuCe0.2-S and (d)CuCe1.0-S catalysts.

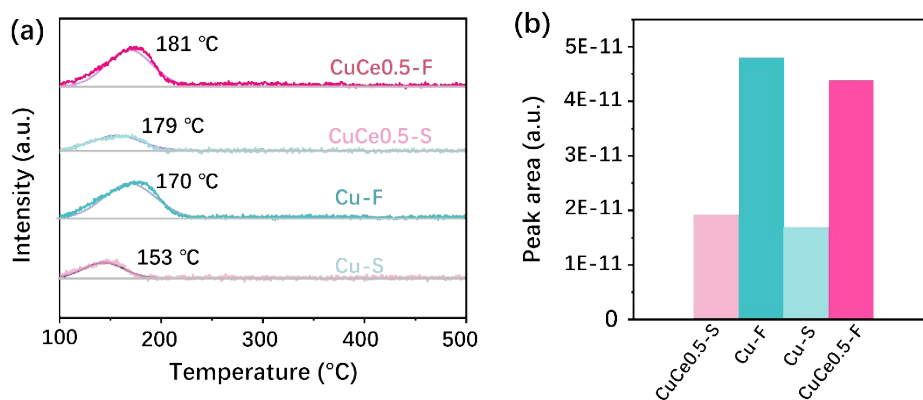


**Fig. S14.** (a) NO+O<sub>2</sub>-TPD profiles of Cu-F, CuCe0.5-F, Cu-S and CuCe0.5-S, and (b) peak area of each catalyst curve. Test conditions: 300 °C pretreatment for 60 min, cooling down to 100 °C, 500 ppm of NO+5 vol.% O<sub>2</sub> gas adsorption for 1h followed by purging in He at 30 mL/min; and heating rate of 10 °C/min to 700 °C.

As shown in the NO+O<sub>2</sub>-TPD (Fig. S14), all catalysts exhibit a clear broad peak of NO desorption in the 200 °C range. Compared to the desorption peak temperature of Cu-F (170 °C), CuCe0.5-F is shifted to a higher temperature of 181 °C. Similarly, the desorption temperature of CuCe0.5-S (179 °C) after sulfidation was higher than that of Cu-S (153 °C). The shift of the desorption temperature of Ce modified zeolites toward higher temperatures was attributed to the enhanced interaction between Cu ions and the SAPO-34, which stabilized the acidic sites on the catalysts. In addition, the peak areas were calculated to compare the relative NO adsorption content on each catalyst. As shown in Fig. S14b, the peak areas of the fresh catalysts are higher than their respective sulfide samples, indicating that sulfur poisoning caused some damage to the adsorption sites of the catalysts leading to a decrease in NO adsorption. The peak area of CuCe0.5-S is higher than that of Cu-S, indicating that Ce can protect the acidic sites on the SAPO-34 framework to a certain extent and stabilize the acidic sites while promoting NO adsorption. The above analysis indicates that Ce can effectively enhance the adsorption of NO by zeolite and thus generate more nitrate compared with the unmodified Cu-SAPO-34.

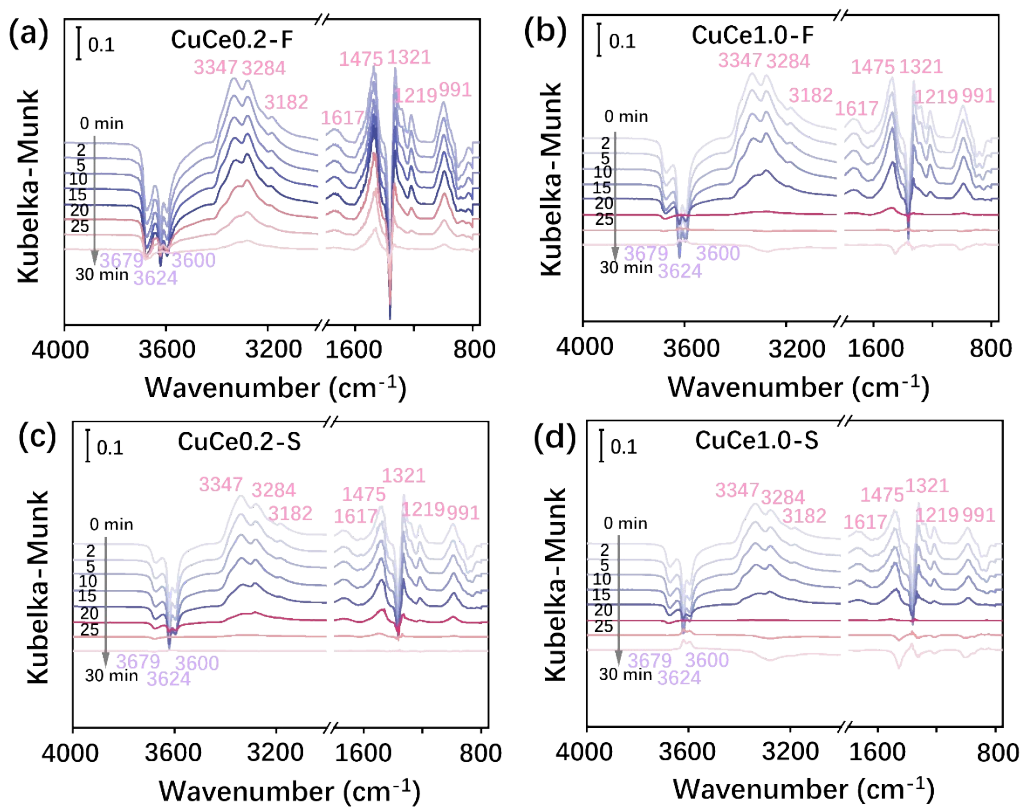


**Fig. S15.** In situ DRIFTS spectra of transient reaction at 200 °C over (a)CuCe0.2-F, (b)CuCe1.0-F, (c)CuCe0.2-S and (d)CuCe1.0-S catalysts between preadsorbed NH<sub>3</sub> and NO+O<sub>2</sub> as a function of time.

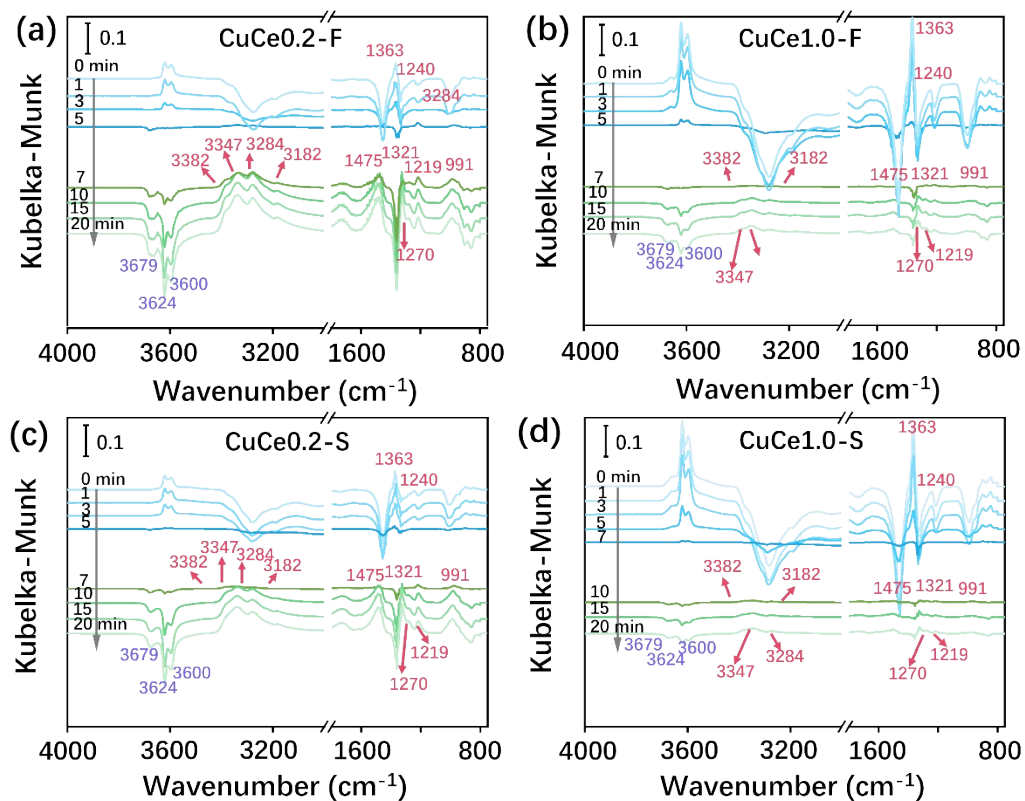


**Fig. S16.** In situ DRIFTS spectra of transient reaction at 200 °C over (a)CuCe0.2-F, (b)CuCe1.0-F, (c)CuCe0.2-S and (d)CuCe1.0-S catalysts between preadsorbed NO+O<sub>2</sub> and NH<sub>3</sub> as a function of time.



**Table S1** Textural parameters of the catalysts obtained from N<sub>2</sub> adsorption-desorption experiments.

<b>Catalysts</b>	<b>Specific surface area (m<sup>2</sup> g<sup>-1</sup>)</b>	<b>Pore diameter (nm)</b>	<b>Pore volume (cm<sup>3</sup> g<sup>-1</sup>)</b>
Cu-F	546	6.41	0.29
CuCe0.2-F	506	5.93	0.27
CuCe0.5-F	440	5.68	0.30
CuCe1.0-F	464	5.16	0.25
Cu-S	441	5.67	0.24
CuCe0.2-S	440	6.87	0.24
CuCe0.5-S	461	5.78	0.26
CuCe1.0-S	412	5.78	0.22

**Table S2** Element content of fresh and SO<sub>2</sub>-poisoned catalysts obtained from ICP-OES results.

<b>Catalysts</b>	<b>Cu (wt.%)</b>	<b>Ce (wt.%)</b>	<b>S (wt.%)</b>	<b>Al (wt.%)</b>
Cu-F	1.64	\	\	13.56
CuCe0.2-F	1.57	0.16	\	13.60
CuCe0.5-F	1.69	0.35	\	13.00
CuCe1.0-F	1.57	0.64	\	12.94
Cu-S	1.86	\	0.38	12.92
CuCe0.2-S	1.84	0.18	0.47	14.47
CuCe0.5-S	1.82	0.43	0.26	13.59
CuCe1.0-S	1.86	0.76	0.24	13.54

## References

1. Y. Zhang, H. Zhu, T. Zhang, J. Li, J. Chen, Y. Peng and J. Li, *Environ Sci Technol*, 2022, 56, 1917-1926.
2. W. Su, Z. Li, Y. Peng and J. Li, *Phys Chem Chem Phys*, 2015, 17, 29142-29149.